Analysis of Structural Stress in 8×8 InSb Array Detector

Qingduan Meng[1,*], Wei Tian[1], Yanqiu Lv[2] and Weiguo Sun[2]

[1]*School of Electronic Information Engineering, Henan University of Science and Technology, Luoyang 471003, China*

[2]*China Airborne Missile Academy, Luoyang 471009, China*

Abstract: Based on viscoplastic Anand's model, structural stress of 8×8 InSb array detector dependent on indium bump sizes is systemically researched by finite element method. For the detector with underfill, simulation results show that as the diameters of indium bump decrease from 36μm to 20μm in step of 2μm, the maximum stress existing in InSb chip first reduces sharply, then increases flatly, and reaches minimum with indium bump diameter 32μm. When the height of indium bump increases from 9μm to 21μm in step of 6μm, the maximal stress in InSb chip first reduces sharply from 800MPa to 500MPa, then almost remains constant. This phenomenon is contrary to the detector without underfill, where the stress is smaller with lower indium height. In the whole device, the maximal Von Mises stress appears in the InSb chip with 10μm, and the minimal Von Mises stress appears in the indium bump array with 16MPa, almost 1/10 of that in underfill encapsulate, where the stress is180MPa. It is noticed that when the Von Mises stress reaches minimum with some selected indium bump dimensions, its stress distribution is uniform and concentrated at all contacting areas, this is favorable to reduce the crack happening in InSb chip, and improve the yield.

Keywords: Finite element method, focal plane array, InSb, structural stress.

1. INTRODUCTION

Indium antimonite (InSb) pn junctions are widely used as infrared photovoltaic detectors and imaging sensors for the 3-5μm spectral range [1, 2]. InSb infrared focal plane array (IRFPA) is usually fabricated by flip chip bonding technology, that is, indium bumps are deposited first on both InSb detector arrays and Si readout integrated circuits (ROIC), then InSb detector array and Si ROIC are aligned and force is applied to cause indium bumps to cold-weld together, as a final processing step in the hybrid fabrication, the InSb substrate is thinned to less than one diffusion length, usually less than 10μm, so that the InSb detector can be illuminated through the backside, and provides high detector quantum efficiency fill factor product, Furthermore, the InSb detector substrate material is thinned to less than 10μm, which is in favor of accommodating the InSb/silicon thermal mismatch for large matrix array. In order to obtain higher signal to noise ratio, InSb IRFPA usually operates at liquid nitrogen temperature (77K), yet stored at room temperature (300K), when its temperature rapidly reduces from 300K to 77K, due to thermal mismatch of the different coefficients of thermal expansion (CTE) of neighboring components, the induced thermal strain and stress are the major causes of breakdown of the detector, such as InSb chip fracture, indium bump crack and delaminating of neighboring materials. In the early stage of flip chip process, there Si chip is connected with FR-4 substrate with SnPb solder joints, both SnPb solder joints crack and delaminating with Si chip or FR-4 substrate

is the main failure pattern. For enhancing the reliability of the flip chip device, underfill is dispensed between Si die and FR-4 substrate; here the underfill participates in the load sharing in parallel with the solder joints, thus lowering the forces that have to be carried by the solder joints due to thermal expansion mismatches. Yet in the InSb IRFPA, the major failure pattern is InSb fracture during rapid temperature drop, which limits the yield of large format detector, so it is necessary to analyze the induced thermal strain and stress values and its distribution in InSb chip. At present time, the thermo-mechanical reliability of flip assemblies is usually assessed by finite element simulations in conjunction with experimental verification, that is, based on the strain and stress analysis, the structure reliability is assessed [3, 4].

In 2009, Rui Wu Chang research group delivered the constitutive relations of indium in extreme-temperature in Anand's model [5], a rate and temperature dependent constitutive model, applied to represent the inelastic deformation behavior of indium at low temperatures down to -150℃. Underfill is an epoxy-based polymer exhibiting time-and-temperature dependent viscoelastic properties. Yet below the glass transition temperature, the underfill is in a glassy state. The glassy underfill is stiff and brittle with high elastic modulus. In this region, the movements of the molecules are restricted. The glass transition temperature of the selected underfill (410K) is larger than 370K, at this temperature, the flip chip process and underfill curing is both completed fully. So in this paper, when the temperature of InSb IRFPA detector is reduced from 370K to 77K, Young's modulus and coefficient of thermal expansion of the selected underfill are considered to be independent of temperature. Thus its viscoelastic properties are reduced to be linear elastic properties.

*Address correspondence to this author at the School of Electronic Information Engineering, Henan University of Science and Technology, Luoyang 471003, China; Tel: +86-379-64231157; office: +86-13525454409; Fax: +86-379-64231910;
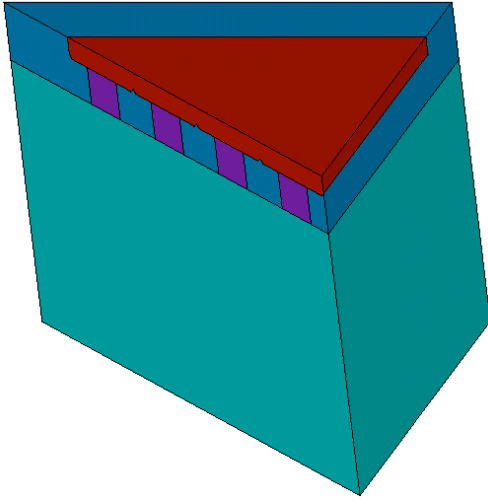E-mail: qdmengly@mail.haust.edu.cn, qdmengly@163.com

Fig. (1). Three dimensional model of infrared focal plane array device.

Table 1. Linaer Elastic Material Parameters

Materials	Elastic Modulus [E/MPa]	Poison's Ratio [μ]	CTE [α1 ppm/K]
Si ROIC	163000	0.28	2.50
InSb chip	409000	0.35	5.04
Indium bump	10600	0.45	33.00
Underfill	9000	0.3	26.00

In this paper, we will demonstrate the effect from indium bump sizes to the structural stress of 8×8 InSb array detector with underfill and without underfill. Basing on the simulated results, the structural stress distribution is obtained.

2. MODEL CREATION AND PARAMETERS SELECTION

When creating the finite element analysis model of InSb IRFPA detector, indium bumps are assumed to be octagonal prisms, and no defects existing in the whole device. InSb IRFPA is composed of InSb photodiode arrays, indium bumps array, Si ROIC and underfill encapsulate materials, just as shown in Fig. (**1**). InSb chip dimensions are 400μm×400μm×10μm, and attached to Si ROIC substrate with 8×8 indium bumps array, Si ROIC substrate dimensions are 500μm×500μm×300μm, indium bump has diameter range of 20~36μm with 50μm pitch, and its height increases from 6μm to 21μm in step of 6μm. Here underfill encapsulate is dispensed between InSb die and Si ROIC substrate for increasing the reliability of flip-chip packaging. In order to describe the mesa structure locating between neighboring detector elements, triangular prisms, whose cross section area sides length are 2.83μm, 2.83μm and 4μm, respectively, are employed. Just as shown in Fig. (**1**). Using the geometrical symmetry, only one eighth of the overall package is modeled. One eighth models contain 6 full and 4 half indium bumps.

InSb chip, Si ROIC substrate and underfill are all considered to be linear elastic materials. All the employed parameters are listed in Table **1**, E is the Young's modulus, μ is the Poisson's ratio, and CTE is the coefficient of thermal expansion. Flip chip process is completed at 370K, at this temperature, no residual stress is assumed to exist within the package. In the simulation, the temperature is gradually reduced from 370K to 77K, which causes thermal stresses to develop. Throughout the temperature drop, no transient heat transfer is considered and the temperature within the model is assumed to be uniform. About 71 seconds increments are taken to lower the temperature to ensure the accuracy. Horizontal displacements normal to the symmetrical surfaces are set to zero, at the same time, the displacement of Si ROIC substrate bottom surface center point remains zero.

Indium bump deformation is strongly temperature and time dependent, and associated with the irreversible, temperature- and rate-dependent inelastic characteristics, which are known to be viscoplastic. Here Anand's viscoplastic constitutive model has been used to describe mechanics of constitutive relationship of indium bump [5-8]. Within the framework of this model, there appears a scalar-valued function for the equivalent plastic strain rate and an evolution equation for the internal variable. Based on the compression test data, the material parameters of indium bump in Anand's model were determined to simulate the steady-state viscoplastic behavior and stress/strain responses [9, 10]. The model accommodates the strain rate dependence on the stress using the following expression

$$\dot{\varepsilon}_p = A \exp(-\frac{Q}{RT})[\sinh(\xi \frac{\sigma}{s})]^{\frac{1}{m}} \tag{1}$$

where $\dot{\varepsilon}_p$ is the inelastic strain rate, A is the pre-exponential factor, Q is the activation energy, R is universal gas constant, T is absolute temperature, m is strain rate sensitivity of stress, ξ is multiplier of stress, s is coefficient for deformation resistance saturation value, and σ is stress. The evolution equation for the internal variable s, which includes the three mechanisms of strain hardening, dynamic recovery, and static recovery, is derived as follows

$$\dot{s} = \{h_0 \left|1 - \frac{s}{s^*}\right|^a sign(1 - \frac{s}{s^*})\}\dot{\varepsilon}_p; a > 1 \tag{2}$$

$$s^* = \hat{s}[\frac{\dot{\varepsilon}_p}{A}\exp(\frac{Q}{RT})]^n \tag{3}$$

Where h_0 is hardening/softening constant, α is strain rate sensitivity of hardening or softening, s* is the saturation value of s, ŝ is the coefficient, and n is the strain-rate sensitivity for the saturation value of deformation resistance. There are nine material parameters in the Anand's model: A, Q, ξ, m, h_0, ŝ, n, a, and s_0, with the last being the initial value of the deformation resistance. As shown in Table **2**.

3. SIMULATION RESULTS ANALYSIS

Temperature of InSb IRFPA is gradually reduced from 370K to 77K in 71 seconds, Von Mises stress distribution of indium bumps is illustrated in Fig. (**2**). For the detector with underfill, just as shown in Fig. (**2a**), the maximal Von Mises stress locating on diagonal indium bump, which has the

Table 2. Material Parameters of Indium for Steady-State Plastic Flow

Material Parameters	Value
A (1/s)	2.33×10^8
Q/R (1/K)	9369.7
ξ	49.97
m	0.30
$\hat{s}$ (N/m^2)	2.83×10^7
n	0
h_0	0
a	1
s_0 (N/m^2)	2.83×10^7

larger distance to neutral point (DNP) on the chip, so has larger induced thermal stress. Besides, the maximal Von Mises stress locating on the contacting area between indium bump and Si ROIC substrate, here the CTE difference is 30.05 ppm/K, has the largest value among all neighboring materials. Yet the maximal Von Mises stress difference (1.4MPa) among indium arrays is so small that the Von Mises stress distribution is assumed to be uniform. For the detector without underfill, just as shown in Fig. (**2b**), for those indium bumps locating on diagonal, Von Mises stress on the contacting areas is apparently concentrated and larger. Yet the maximal Von Mises stress appears on the contact area between indium bumps and InSb chip, this is contrary to the device with underfill, just as shown in Fig. (**2a**), where the maximal stress appears on the contacting area between indium bump and Si ROIC substrate, where the biggest coefficient of thermal expansion mismatch exists. The maximal stress location changes from indium bump bottom surface to top surface. For this thinner indium bump thickness (10μm) is used, as the indium bump height changes from 21μm (with underfill) to 9μm (without underfill), its thermal mismatching absorbing capacity reduces, thus the maximal Von Mises stress will transfer from indium bump bottom surface to top surface.

In order to learn the effect from the indium bump diameter to Von Mises stress and its distribution in InSb chip, here a typical structure with InSb thickness 10μm is selected. Taking account of manufacturing precision, it reduces the diameters of indium bump from 36μm to 20μm in step of 2μm, simulation results are shown in Fig. (**3**). For the detector with underfill, just as shown in Fig. (**3a**), when indium bump height is fixed at 9μm, the maximal Von Mises stress in the InSb chip reduces sharply from 1000MPa to 752MPa, then increases flatly to 810MPa with reduced indium bump diameters. When indium bump height is fixed at 15 or 21μm, the maximal Von Mises stress in the InSb chip versus indium bump diameters almost has the same varying tendency, just like the curve is shifted down at some values. When the height of indium bump increases from 9μm to 21μm in step of 6μm, the maximal stress in InSb chip first reduces sharply from 800MPa to 500MPa, then fluctuates at 500 MPa, it seems that the maximal stress in InSb chip does not reduce. It is worth noticing that when the diameter of the indium

bump is set to 32μm, the maximum stresses existing in InSb chip reached the minimum, this phenomena has nothing to do with indium standoff height. Von Mises stress distribution on InSb chip bottom is shown in Fig. (**4a**). For the detector without underfill, just as shown in Fig. (**3**) b,when indium bump height is fixed 21 μm, the maximal von Mises stress in the InSb chip reduces linearly firstly from 199 MPa to 122 MPa, then increases to 182 MPa with reduced indium bump diameters. It is worth noticing that when indium bump height is fixed 9 μm, the maximal Von Mises stress in the InSb chip increases firstly from 52 MPa to 75 MPa, then decreases linearly to 54 MPa with reduced indium bump diameters. When the diameter of the indium bump is set to 28 μm, the maximum stresses in InSb chip reached the maximum. Apparently the Von Mises stress dependent on indium bump diameter in the detector without underfill contrary to that happening in the detector with underfill, here when the height of indium bump increases from 9μm to 21μm in step of 6μm, the maximal stress varying tendency versus indium diameters is just like the inverted letter V that evolves to the letter M, then to the letter V, its Von Mises stress distribution on InSb chip bottom is shown in Fig. (**4b**).

Apparently, for the detector with underfill, Von Mises stress existing on contact areas between InSb chip and indium bumps is concentrated and uniform, its stress value is about 300Mpa, larger than that of its surrounding areas. The maximal stress value about 600MPa situates at the edge far away from neutral point, where the InSb chip is confined by its surrounding underfill encapsulant and does not shrink freely. The minimal stress value about 60MPa locates on the trough intersection zones. There is an obvious stress gradient from contact section center to non-contact region. For the detector without underfill,Von Mises stress existing on contact areas between InSb chip and indium bump is also apparently concentrated and uniform, its value is about 40 MPa, much smaller than that with underfill, and the stress existing on non-contact areas fluctuates around 15 MPa. There is an obvious stress gradient from contact section to non-contact region, and the stress value of contact areas along diagonal is larger than other's. For the detector with underfill ,Von Mises stress distribution in Si ROIC is almost concentrated strongly on the contacting areas between indium bumps and Si ROIC, besides, on the quadrilateral borders of Si ROIC top surface, there are several non-continuous spots where Von Mises stress id largest, especially on the corner of Si ROIC top surface, just as shown in Fig. (**5a**). Yet for the detector without underfill, Von Mises stress existing on contact areas between Si ROIC and indium bump also is concentrated and uniform, its value is also about 20 MPa, and the stress existing on non-contact areas is negligible.

The Temperature of 8×8 InSb IRFPA drops from 370K to 77K. Von Mises stress distribution in underfill is shown in Fig. (**6**). On the whole region under InSb chip, the stress distribution is uniform, but around indium bump octahedral shell, the stress is apparently enlarged. At the four corners of underfill top surface, Von Mises stress is smallest, here the underfill can shrink freely, as for the four corners of underfill bottom surface, Von Mises stress enlarged for underfill is
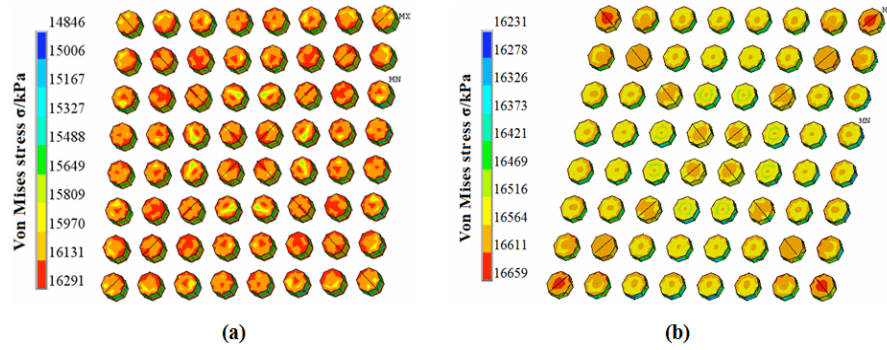
Fig. (2). Von Mises stress distribution of indium bump array (**a**) with and (**b**) without underfill.
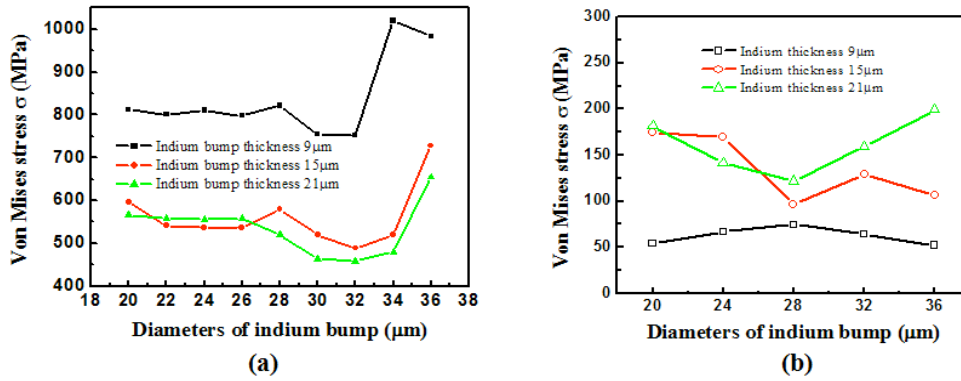

Fig. (3). Maximum stress values of InSb as a function of indium bump diameter with different indium bump heights (**a**) with and (**b**) without underfill.
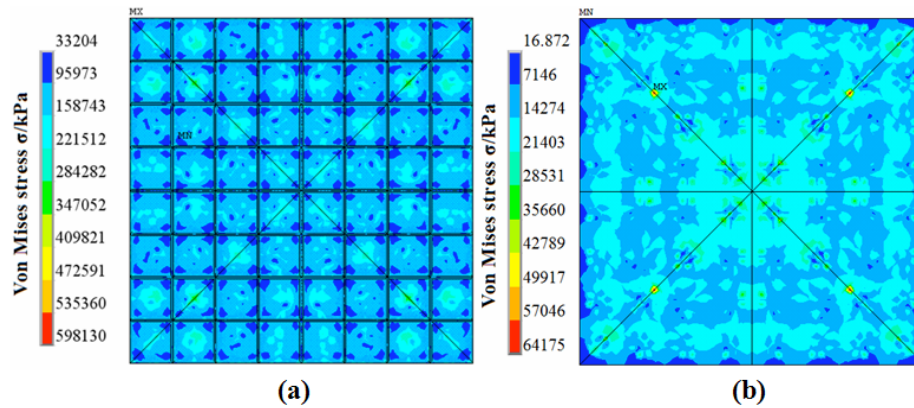

Fig. (4). Von Mises stress distribution of InSb chip bottom surface (**a**) with and (**b**) without underfill.
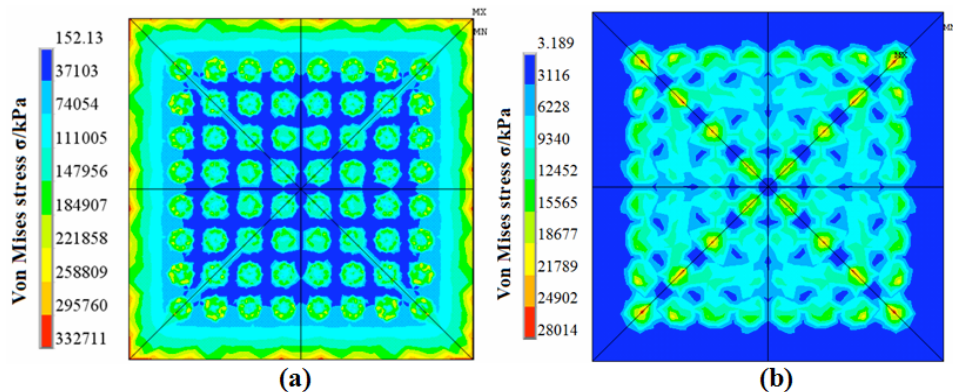

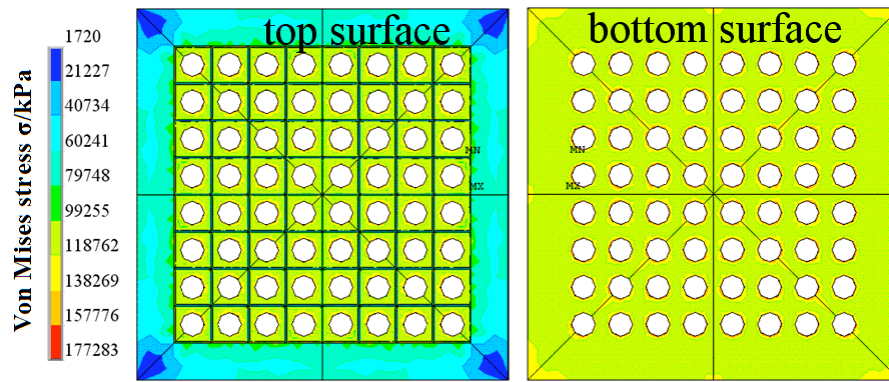**Fig. (5).** Von Mises stress distribution of Si ROIC (**a**) with and (**b**) without underfill.

Fig. (6). Von Mises stress distribution of underfill.

glued with Si ROIC. Besides, the maximal Von Mises stress in the underfill encapsulate seems to have nothing to do with indium bump diameters, and fluctuates at 180MPa.

In conclusion, for the detector with underfill, Von Mises stress in 8×8 InSb infrared focal plane array, about 500MPa, appears on InSb chips edges, which is farthest to the neutral point, the minimal Von Mises stress, about 17MPa, locating in indium bump array, and the stress in underfill encapsulant is about 180MPa, almost 10 times of that in indium bump array, this is not proportional to the support area, though their Young's modulus, Poisson's ratio, and coefficient of thermal expansion are comparable. All these are distinct from the Von Mises stress distribution in 8×8 InSb array detector without underfill, where the Von Mises stress distribution in all the contacting areas is uniform and concentrated, and its maximal stress is also located in contacting area between InSb chip and indium bump.

4. CONCLUSIONS

Crack appearing in the InSb chip limited the InSb IRFPA yield. Based on finite element analysis, impacts on Von Mises stress and its distribution in the InSb IRFPA from both indium bump diameters and heights are completely discussed in this manuscript. For the detector with underfill, simulation results show that as the indium bump diameter and standoff height are set to 32μm and 21μm.respectively, the maximal Von Mises value existing in InSb chip reaches minimal values 458MPa, and its stress distribution is uniform at contacting areas between InSb chip and indium bump. Yet for the detector without underfill, when the height of indium bump is set at lower value, such as 9μm, the maximal Von Mises value existing in InSb chip reaches minimal values 50MPa, and its stress distribution is uniform contacting areas between InSb chip and indium bump. It seems that the stress is smaller with lower indium height for

the detector without underfill, yet for the detector with underfill, it seems that the stress is smaller with higher indium height. So indium bump height is a crucial parameter for reducing thermal stress in InSb IRFPA detector.

REFERENCES

[1]   Y. Gau, L. Dai, S. Yang, P. Weng, K. Huang, Y. Liu, C. Chiang, F. Jih, Y. Cherng, and H. Chang "256×256 InSb Focal Plane Arrays," *Proceedings of SPIE*, vol. 4078, pp. 467-479, 2003.
[2]   W. Parrish, J. Blackwell, G. Kincaid, and R. Paulson, "Low-Cost High Performance InSb 256 × 256 Infrared Camera", *Proceedings of SPIE*, vol. 1540, pp. 274-284, 1991.
[3]   J. Pang and D. Chong, "Flip chip on board solder joint reliability analysis using 2-D and 3-D FEA models", *IEEE T. Adv. Packaging*, vol. 24, pp. 499-506, 2001.
[4]   Z. Zhang and C. P. Wong, "Recent advances in flip-chip underfill: Materials, process, and reliability", *IEEE T. Adv. Packaging*, vol. 27, pp. 515-523, 2004.
[5]   R. Chang and F. Patrick Mccluskey, "Constitutive Relations of Indium in Extreme Temperature Electronic Packaging Based on Anand Model", *J. Electron. Mater.*, vol. 38, pp.1855-1859, 2009.
[6]   S. Kim and H. Ledbetter, "Low-temperature elastic coefficients of polycrystalline indium", *Mater. Sci. Eng., A*, vol. 252, pp.139-143, 1998.
[7]   E. Hermida, D. Melo, J. Aguiar and D. Lopez, "Temperature dependence of the viscoelastic response of In, Sn and In-Sn alloys", *J. Alloys Compd.*, vol. 310, pp. 91-96, 2000.
[8]   R. Reed, C. McCowan and R. Walsh, "Tensile strength and ductility of indium", *Mater. Sci. Eng.*, vol. 102, pp.227-236, 1988.
[9]   G. Wang, Z. Cheng, K. Becker and J. Wilde, "Applying anand model to represent the viscoplastic deformation behavior of solder alloys", *J. Electron. Packaging*, vol. 123, pp.247-253, 2001.
[10] J. Wilde, K. Becker, M.Thoben, W. Blum, T.Jupitz, G. Wang and Z. Cheng, "Rate dependent constitutive relations based on Anand model for 92.5Pb5Sn2.5Ag solder", *IEEE T. Adv. Packaging*, vol. 23, pp.408-414, 2000.